Supplementary Information

Catalytic Dioxygen Reduction Mediated by a Tetranuclear Cobalt Complex Supported on a Stannoxane Core

Anirban Chandra[a], Stefan Mebs[b], Subrata Kundu[a], Uwe Kuhlmann[c], Peter Hildebrandt[c], Holger Dau[b], Kallol Ray*[a]

[a]Humboldt-Universität zu Berlin, Institut für Chemie, Brook-Taylor-Straße 2, D-12489 Berlin (Germany). [b]Freie Universität Berlin, FB Physik, Arnimallee 14, D-14195-Berlin (Germany); [c]Department of Chemistry, Technische Universität Berlin, Straße des 17. Juni 135, 10623 Berlin (Germany).

 * kallol.ray@chemie.hu-berlin.de

Supporting Information

Table of Contents

Experimental Section

1. Materials

All chemicals were purchased from Sigma-Aldrich, Acros, ABCR, TCI and used without further purification unless otherwise mentioned. Anhydrous solvents (dichloromethane, acetone, ethyl acetate) were purchased from Carl-Roth GmbH ($\geq$ 99.5%, < 50 ppm H_2O) and degassed by freeze-pump-thaw method prior to use. $^{18}O_2$ (97 atom %) was purchased from Sigma-Aldrich. Tetranuclear stannoxane ligand and it's cobalt(II) complex were prepared by following the literature procedures.[S1] The substrates used in kinetic experiments were purified using standard methods.[S2] All the liquid substrates for reactivity studies were distilled under argon prior to use.

2. Instrumentation and Physical methods

Preparation and handling of air sensitive materials were performed in a N_2 glove box OMNI-Lab 2 (VAC) with O_2 and moisture concentrations less than 1 ppm. ^1H NMR spectra were recorded either on a Bruker AV 400 NMR spectrometer or on a Bruker DPX 300 spectrometer. Elemental analyses were performed with a Leco CHNS-932 elemental analyser. UV-Vis spectra were recorded by Agilent 8453 diode array spectrometer connected with a cryostat from Unisoku Scientific Instruments, Japan. IR spectra were measured either from KBr pellets with a Shimadzu FTIR-8400S spectrometer or by dropping the sample solution on an ATR unit (diamond) connected to a Bruker Vector 22 spectrometer. Resonance Raman (rRaman) spectra were measured at -80 °C (Bruker cryostat) with 514-nm excitation, by using a Horiba Jobin-Yvon LabRAM HR800 confocal Raman spectrometer.

X-Band EPR spectra were recorded on a Bruker ELEXYS E580 X-band EPR spectrometer equipped with the Bruker ER4118X-MD5 probe head, and an Oxford Instruments CF935 helium flow cryostat. The freshly prepared samples were transferred to J. Young quartz EPR tubes and sealed. The solution in the tube was frozen in liquid nitrogen and kept frozen until measured.

Crystal Structure Determination:

Data collection was performed at 100 K on a Stoe IPDS 2T diffractometer using Mo-K radiation ($\lambda = 0.71073$ Å); radiation source was a sealed tube generator with graphite monochromator. Multi-scan (PLATON [S3a]) absorbtion correction for **L1 (CCDC 818335)** and numerical absorbtion correction were performed. The structures were solved by direct methods (SHELXS-97 [S3b]) and refined by full matrix least-squares procedures based on F^2 with all measured reflections (SHELXL-97 [4]). All non-hydrogen atoms were refined anisotropically. H atoms were introduced in their idealized positions and refined as riding.

XAS/DFT measurement:

XAS measurements were conducted at the KMC3 beamline of the BESSY synchrotron at the Helmholtz-Zentrum Berlin (HZB). The samples were disposed at ca. -60°C into cylindrical Teflon sample holders with thin walls of roughly 100 μm specifically designed for X-ray spectroscopy. Data collection was performed at 20 K in a liquid-helium cryostat in fluorescence detection mode using a 13 element ultra-low energy resolving Silicon drift detector (SDD) from Canberra. Over 25 spectra were averaged for each compound in order to improve the signal-to-noise ratio. Averaged spectra were background-corrected and normalized using in-house software. Subsequently, unfiltered k^3-weighted spectra and phase functions from FEFF8.5[S5] were used for least-squares curve-fitting of the EXAFS with in-house software and for calculation of Fourier-transforms representing k-values between 2 and 14 Å^{-1}. Data were multiplied by a fractional cosine window (10% at low and high k-side); the amplitude reduction factor S_0^2 was 0.95. The structural models for the phase function computations were obtained by DFT optimization of the dimer structure (resembling **1**) at the UB3PW91/ 6-31+G*[S7] level of theory (an effective core potential was used for Co[S8]) applying Gaussian16[S9].

To investigate the nature of **Co$_4$L1**, DFT calculations on the same level of theory were conducted for six small model compounds, see Figure S4. Like for the calculation of the **1** model, the COSMO solvation model was used to mimic the acetone solvation[S10]. Dispersion was implemented by the empirical disperison correction of Grimme[S11]. Subsequent to geometrical optimizations, normal mode analysis (frequency calculation) was carried out to check if the structures are local minima of the potential energy hypersurface. Model 1 (with one acetone and one triflate) exhibits

one virtual vibration of -6.7 cm⁻¹, which accords to a low-energy phononic-type of general motion and doesn't alter the structure/energy in any considerable fashion, so no efforts were made to reoptimize the structure. Model 2 shows three virtual vibrations at -49.4, -25.5, and -8.1 cm⁻¹, all of which break the imposed Cs-symmetry. This model serves as reference (effect of symmetry constraints) and wasn't expected to be the true structure of compound **Co₄L1**. Models 3-6 are local minimum structures.

The electronic structure of DFT model 5 (resembling **Co₄L1**) was studied in detail applying a variety of Real-Space Bonding Indicators (RSBIs) derived from the Atoms-In-Molecules (AIM)[S12], Non-Covalent Interactions index (NCI[S13]), and Electron Localizability Indicator (ELI-D[S14]) methods. By definition of surfaces of zero electron flux AIM provides atomic basins as well as a topological bond paths motif which resembles the molecular structure. ELI-D divides space into small regions carrying equal amounts of same-spin electron pairs, thus providing basins of paired core, bonding or lone pair electrons. By mapping the reduced density gradient, $s(\mathbf{r}) = [1/2(3\pi^2)^{1/3}]\cdot|\nabla\rho|/\rho^{4/3}$, at specific *iso*-values NCI uncovers regions in space where non-covalent interactions occur. NCI complements ELI-D analysis, since the latter is closely related to covalent bonding. Mapping the ED times the sign of the second eigenvalue of the Hessian ($\text{sign}(\lambda_2)\rho$) on *iso*-surfaces of $s(\mathbf{r})$ facilitates the assignment of different contact types including steric/repulsive ($\lambda_2 > 0$), non-bonding ($\lambda_2 \approx 0$), and (weakly) attractive ($\lambda_2 < 0$). Topological analysis of the electron density was performed using AIM2000[S15], whereas ELI-D related real-space bonding descriptors were generated and analyzed with DGRID[S16] (grid step size of 0.15 au). NCI grids were computed with NCIplot[S17] (grid step size of 0.10 au). Bond paths are displayed with AIM2000, ELI-D and NCI figures are displayed with MolIso.[S18]
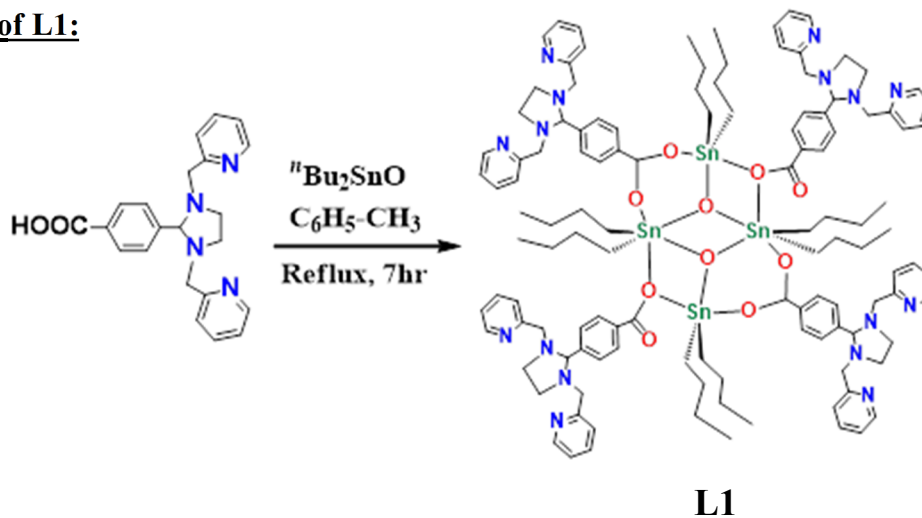
3. Synthesis of Ligand and metal-complex

3.1. Synthesis of L0
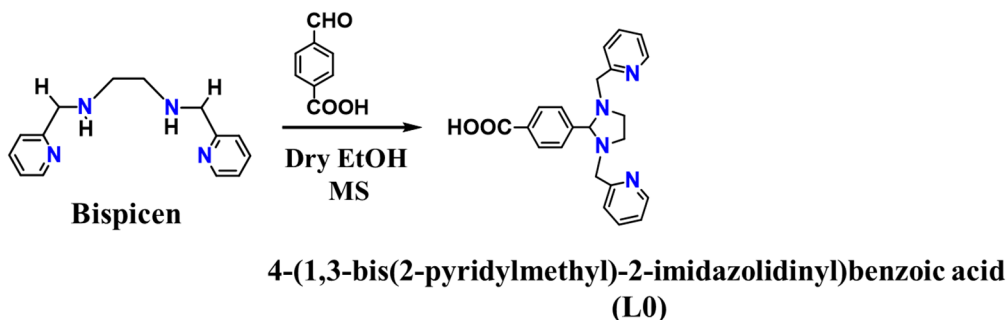
Scheme S1: Preparation of **L0** from bispicen

N,N'-Bis(pyridin-2ylmethyl)-ethane-1,2-diamine (bispicen) and 4-(1,3-bis(2-pyridylmethyl)-2-imidazolidinyl)benzoic acid (L0) was prepared according to the reported method.[S1a][S1c]

3.2. Synthesis of L1:

Scheme S2: Preparation of **L1** from **L0**

Synthesis of L1: di-*n*-butyltin oxide, *n*Bu$_2$SnO (0.66 g, 2.67 mmol) was added to a suspension of 4-(1,3-bis(2-pyridinylmethyl)-2-imidazolidinyl)benzoic acid **(L0)** (1.00 g, 2.67 mmol) in anhydrous toluene (80 mL) and the reaction mixture was refluxed at 120 - 130 °C with continuous removal of water by using a Dean-Stark apparatus. After 7 hours, the reaction mixture was allowed to cool to room temperature and then filtered. The solvent from the filtrate was removed under reduced pressure. The expected product was recovered as a pale yellow solid.

Yield: 80.1%

Single crystals of **L1** suitable for X-ray crystallography were grown by slow evaporation of a concentrated solution of **L1** in toluene.

Melting point: 261 °C (decomposed).

NMR: ^{119}Sn NMR (CDCl$_3$, 150 MHz): δ (ppm) -210.82 (s) and -213.81 (s).

^{1}H NMR (CDCl$_3$, 400 MHz): δ (ppm) 8.48 (m, 8H, *H*-Ar), 8.04-7.93 (m, 8H, *H*-Ar), 7.75-7.62 (m, 16H, *H*-Ar), 7.15-6.98 (m, 16H, *H*-Ar), 4.15 (s, 4H, C*H*), 4.09-3.95 (m, 16H, C*H*$_2$-py), 3.51-3.28 (m, 16H, C*H*$_2$-N), 1.61-1.05 (m, 48H, C*H*$_2$), 0.92 (t, 24H, C*H*$_3$).

IR (KBr): (in cm^{-1}) = 3445 br, 3062 w, 3008 w, 2955 s, 2925 m, 2868 m, 2816 w, 1611 s, 1605s, 1593 s, 1569 s, 1546 s, 1475 m, 1432 s, 1403 s, 1340 s, 1290 m, 1157 m, 1129 m, 1081 w, 1018 s, 867 m, 783 s, 757 w, 710 m, 685 s

3.3. Synthesis of Co$_4$L1:

A solution of **L1** (0.50 g, 0.2 mmol) in anhydrous acetone (2 mL) was added to a suspension of Co^{II}(OTf)$_2$ (0.290 g, 0.8 mmol) in anhydrous acetone (4 mL). The light orange reaction mixture was stirred in anhydrous conditions, under nitrogen at room temperature for 24 hours. The solution was then filtered. After the addition of 40 mL of anhydrous *n*-hexane to the filtrate, **Co$_4$L1** precipitated as a dark-yellow powder. The remaining solvent was removed by decantation and **Co4L1** was dried in high-vacuum overnight.

Elemental analysis: C$_{128}$H$_{160}$Co$_4$F$_{24}$N$_{16}$O$_{34}$S$_8$Sn$_4$ Calculated (%): C, 39.52; H, 4.15; N, 5.76. Found (%) C, 38.82; H, 4.35; N, 5.56

IR (KBr): (in cm^{-1}): 3265 br, 3050 w, 2958 s, 2923 s, 2856 s, 2323 s, 2093 s, 1705 s, 1624 s, 1615 s, 1605 s, 1591 m, 1572 m, 1549 m, 1463 s, 1404 s, 1378 s, 1344 m, 1281 w, 1259 s, 1225 s, 1158 s, 1080 s, 1032 s, 871 s, 797 s, 752 w, 700 m, 685 s.

X-band EPR: effective $g'_\perp$ = 4.01 and $g'_\parallel \approx 2.0$

3.4. Generation of the 1:

Under inert conditions, a pale yellow solution of the complex **Co₄L1** in anhydrous acetone (0.5 mM, 2 mL) was kept at -50 °C. Anhydrous O_2 was then bubbled into the solution. The formation of a deep orange intermediate was monitored following the growth of the 464 nm band in the UV-vis spectrum.

UV-vis (acetone, -50 °C): λ_{max} (ε_{max}) 464 nm (12,232 $M^{-1}cm^{-1}$).

X-band EPR: Silent

-210.8:
-213.8

ppm (t1) -175   -200   -225   -250   -275
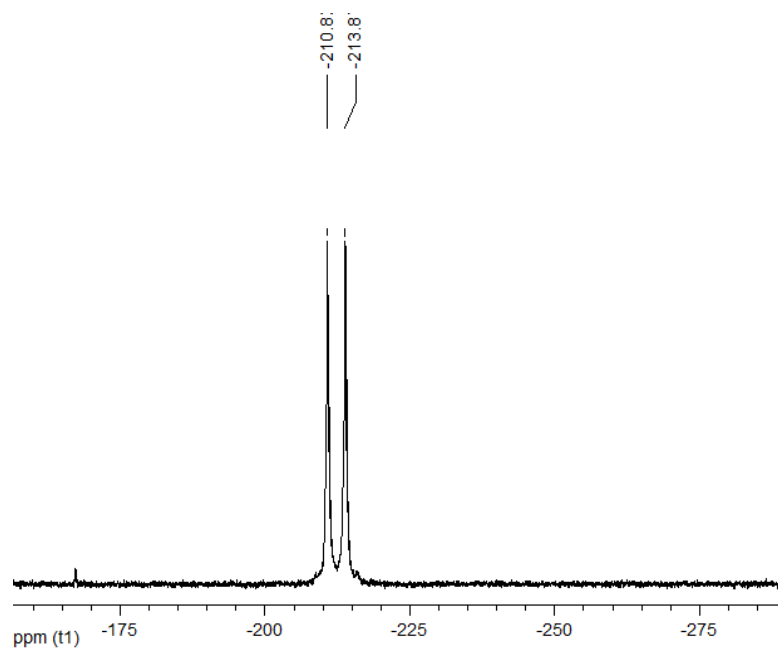
Figure S1. ^{119}Sn NMR spectrum of **L1** in CDCl$_3$ at 25 °C.
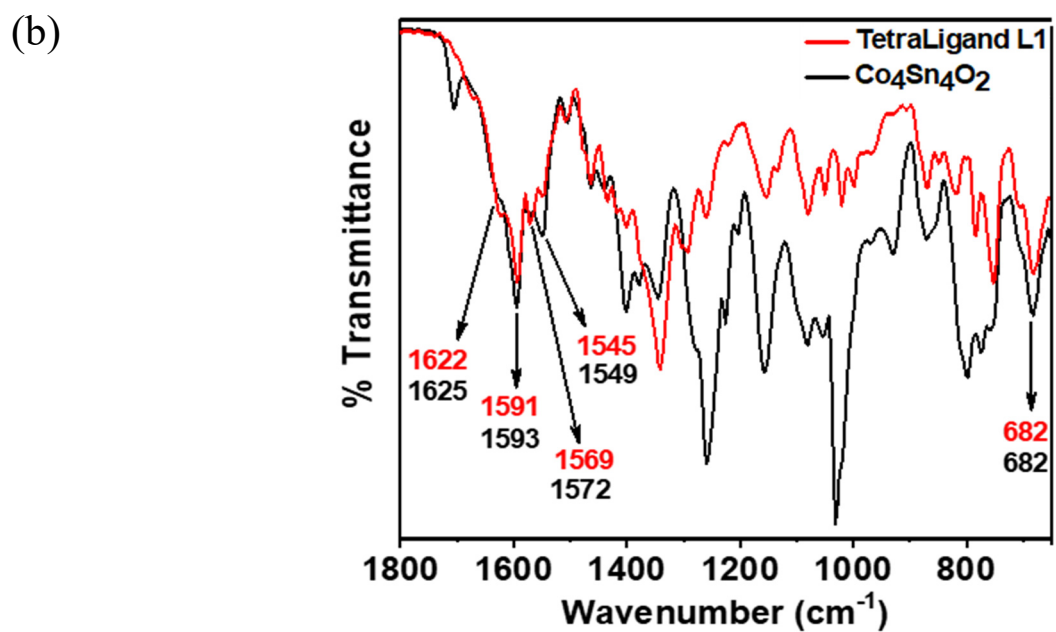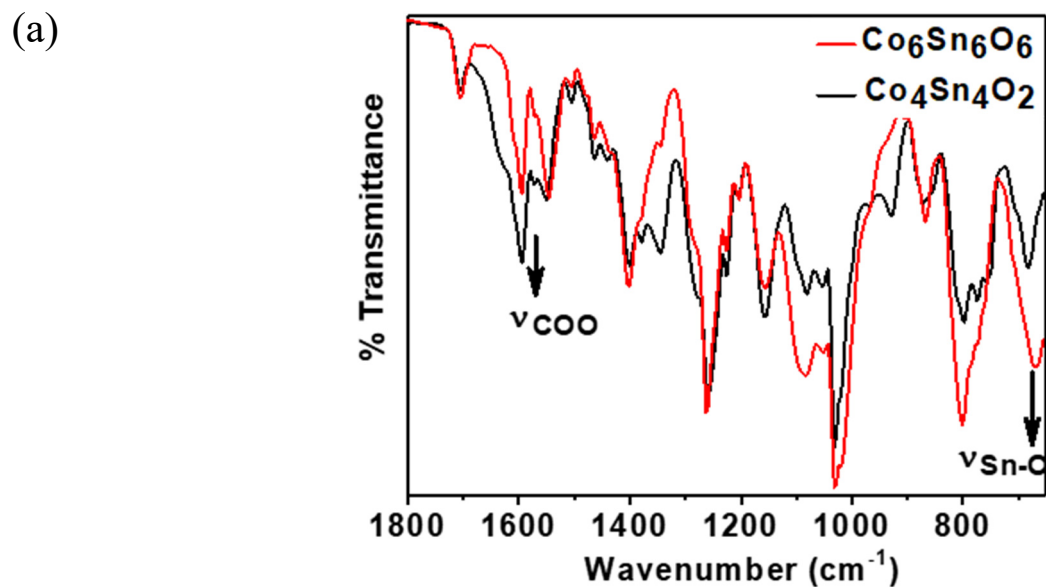
(a)

(b)

Figure S2. (a) Comparison between the FTIR spectra of cobalt complexes having Hexameric and Tetrameric Stannoxane ligand. (b) Comparison between the FTIR spectra of Stannoxane ligand **L1** and **Co₄L1**: vibration frequencies are shown for **L1** (red color) and **Co₄L1** (black color)
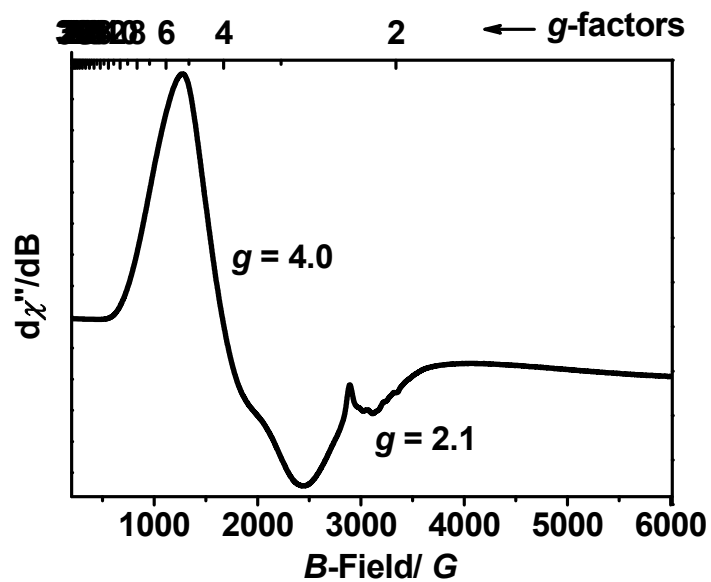
Figure S3. EPR spectra of complex **Co₄L1** in Acetone, concentration 2 mM. This spectrum was acquired at 13.5 K, MWFQ = 9.354355 GHz, using a power of 2.00 mW and a field modulation amplitude of 5.002 G.
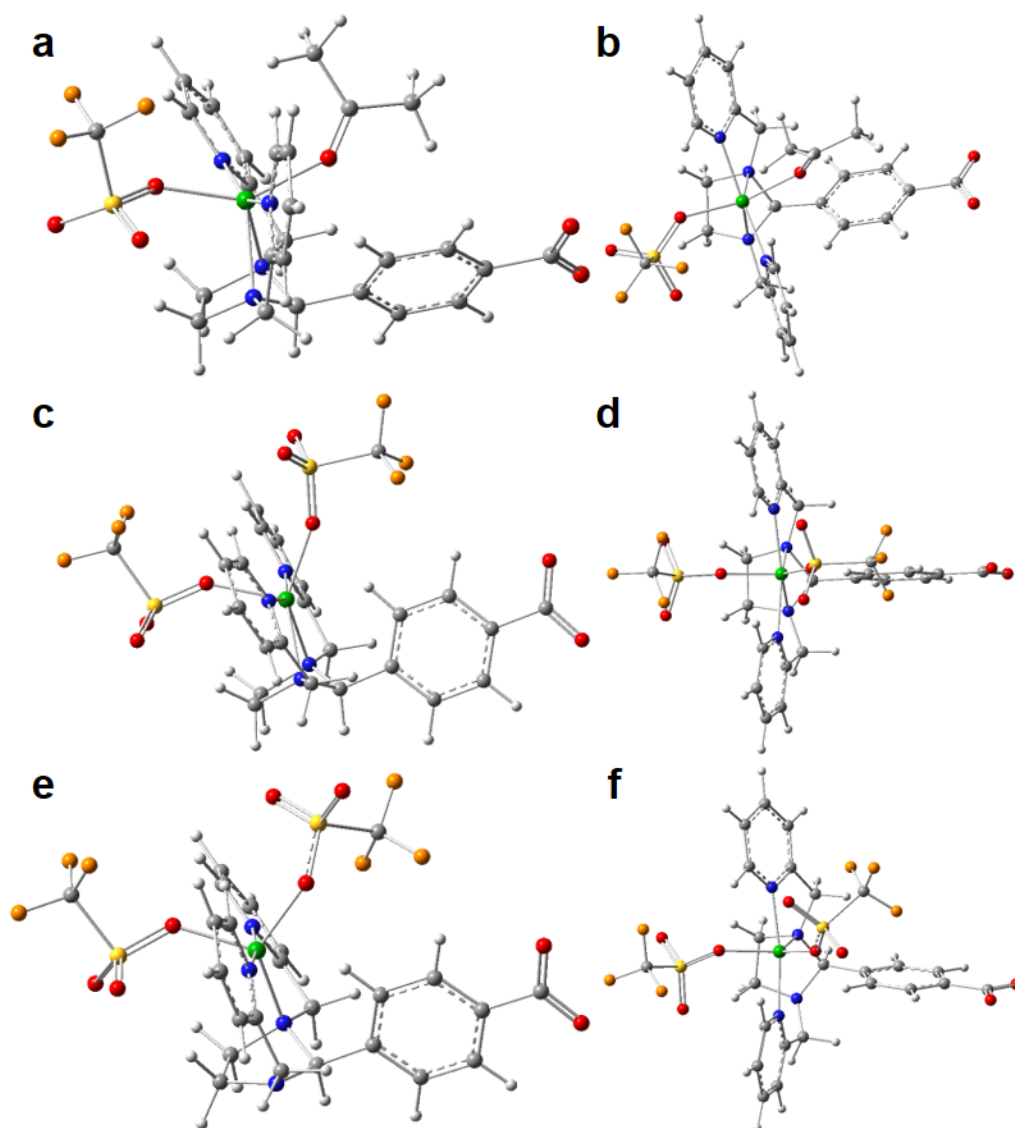
Figure S4a. Side view (left column) and top view (right column) of DFT models 1-3 optimized at the uB3PW91/6-31+G* level of theory and including COSMO solvation model (acetone) and empirical dispersion correction, see text.

Model 1 comprises one triflate anion and one acetone solvent molecule in *trans*-like arrangement as coordinating ligand; model 2 has two triflate anions under the restriction of Cs-symmetry; model 3 is equal to model 2, but without symmetry restriction.
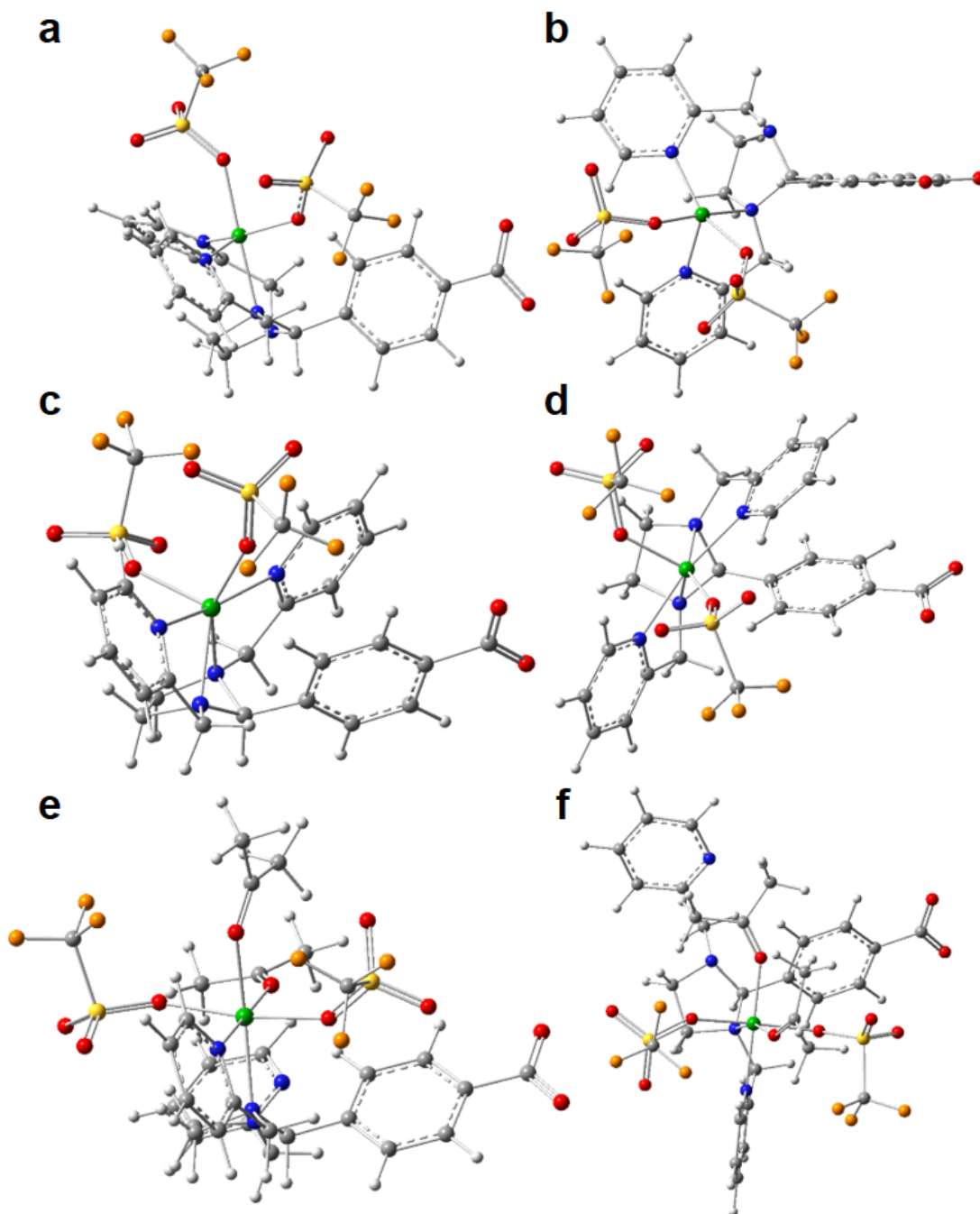
Figure S4b. Side view (left column) and top view (right column) of DFT models 4-6.

Model 4 has two triflate anions in *cis*-like arrangement; model 5 is related to model 3, but shows less symmetric ligand binding; model 6 considers the potential coordination of two triflate anions and two acetone solvent molecules.

Table S1. Calculated Co–X (X = N,O) distances of the unprotonated (COO⁻) and the protonated (COOH) DFT models 1-6 (in Å) resembling **Co₄L1**, and the dimer model resembling **1**.

COO-	O	O'	Nⁱ	Nⁱ"	Nᵖ	Nᵖ'	d(av)
1	2.14	2.11	2.25	2.17	2.11	2.16	2.16
2	2.15	2.13	2.24	2.24	2.19	2.19	2.19
3	2.04	2.07	3.30	2.10	2.11	2.14	2.09
4	2.16	2.03	3.60	2.18	2.07	2.03	2.09
5	2.15	2.07	2.23	2.27	2.25	2.19	2.19
6	2.12	2.13	2.14	2.05	2.22	2.09	2.13

COOH	O	O'	Nⁱ	Nⁱ"	Nᵖ	Nᵖ'	d(av)
1	2.15	2.10	2.25	2.18	2.12	2.16	2.16
2	2.14	2.12	2.25	2.25	2.19	2.19	2.19
3	2.04	2.07	3.31	2.10	2.12	2.14	2.09
4	2.16	2.03	3.56	2.16	2.08	2.04	2.09
5	2.14	2.07	2.21	2.29	2.25	2.19	2.19
6	2.12	2.12	2.13	2.06	2.24	2.09	2.12

1	Otf	OO	Nⁱ	Nⁱ"	Nᵖ	Nᵖ'	d(av)
19-Co-8	1.97	1.81	1.92	3.37	1.95	1.92	1.92
19-Co-55	1.97	1.80	1.95	3.27	1.96	1.91	1.92

Color code is included to guide the eye. Model 6 has four O-atom and two N-atom ligands. For the 5-coordinate models 3 and 4 the long Co–N distance was not included in the averaging. The effect of protonation of the carboxylate group is negligible.

Table S2.   Absolute and relative molecular energies of DFT models 1-6 (unprotonated).

model	energy	delta	kJ/mol	model	energy	delta	kJ/mol
1	-2520.475			**1**+a+t	-3674.969	0.006	16.1
2	-3288.748	0.012	31.4	**2**+2a	-3674.963	0.012	31.4
3	-3288.758	0.002	5.2	**3**+2a	-3674.973	0.002	5.2
4	-3288.741	0.019	51.2	**4**+2a	-3674.955	0.019	51.2
5	*-3288.760*	*0.000*	*0.0*	*5+2a*	*-3674.975*	*0.000*	*0.0*
6	-3674.991			**6**	-3674.991	-0.016	-41.4
				acetone	-193.107		
				triflate	-961.386		

Energy differences are referenced to model 5 (*italic*), which is the energetic minimum of this model type (CoL(OTf)$_2$). For an overall comparison/estimate of the relative molecular energies, the different DFT model types have been "filled up" by acetone (a) and/or triflate (t) molecules calculated independently.
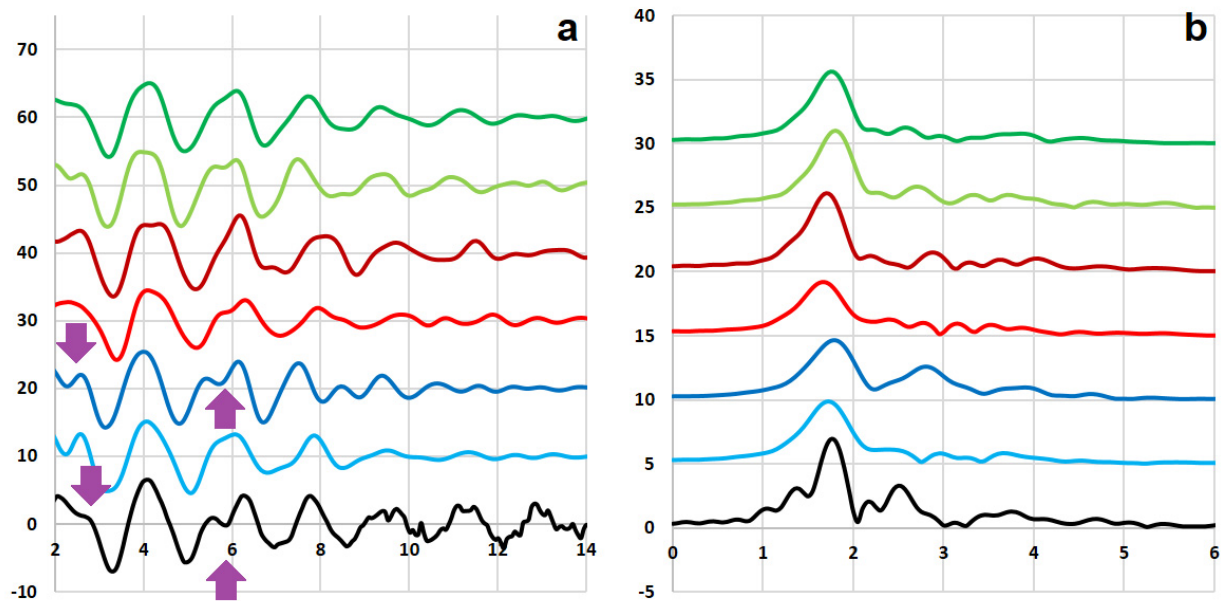
Figure S5. a) k^3 weighted EXAFS and b) FT of EXAFS of DFT models 1 (dark green), 2, (light green), 3 (dark red), 4 (light red), 5 (dark blue), 6 (light blue), and experimental data of compound **Co₄L1** (black). The purple arrows are included to guide the eye towards similarities between DFT spectrum of model 5 and the experimental data of **Co₄L1**.
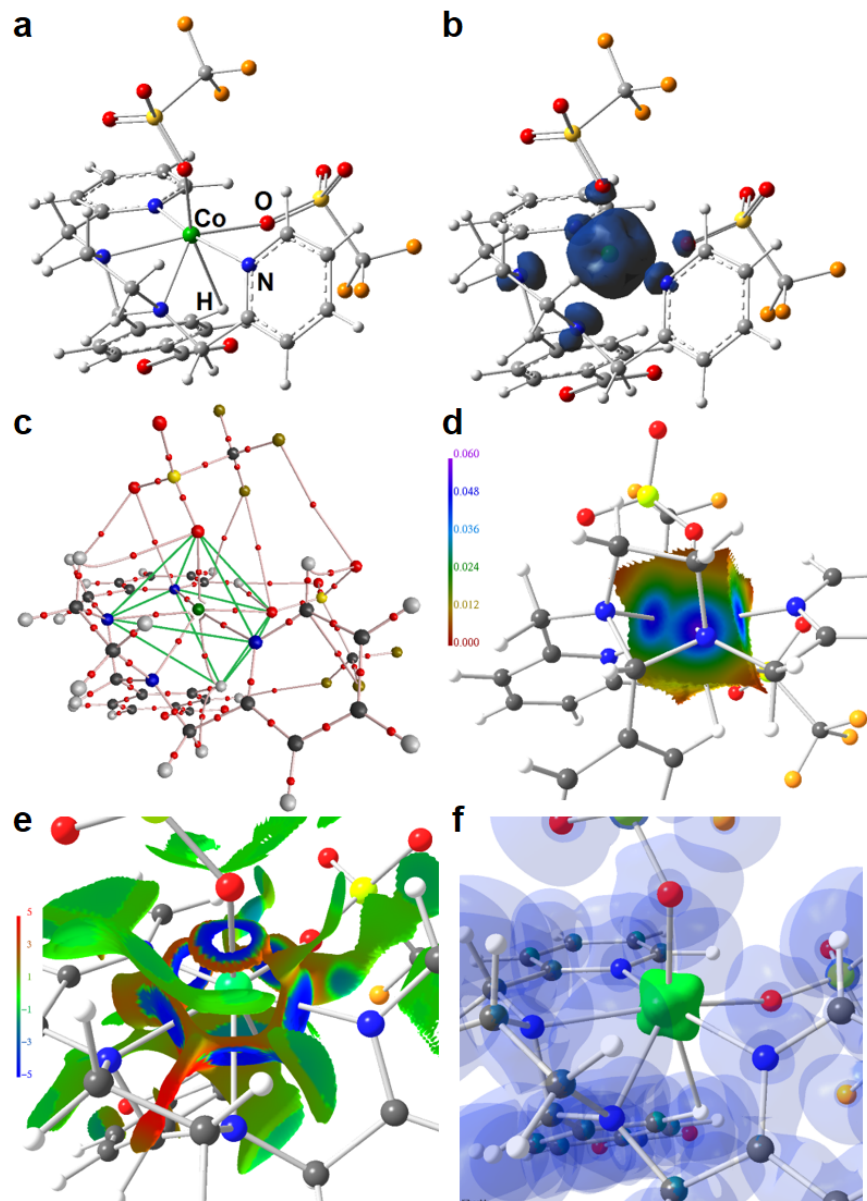
Figure S6. (a) DFT optimized structure of model 5, (b) Spin density *iso*-surface at 0.005 a.u. (c) AIM-topology (straight green lines are introduced to guide the eye), (d) Electron density distribution mapped on the AIM basin of the Co atom, (e) NCI *iso*-surface at s(**r**) = 0.5, (f) ELI-D *iso*-surface at γ = 1.3.

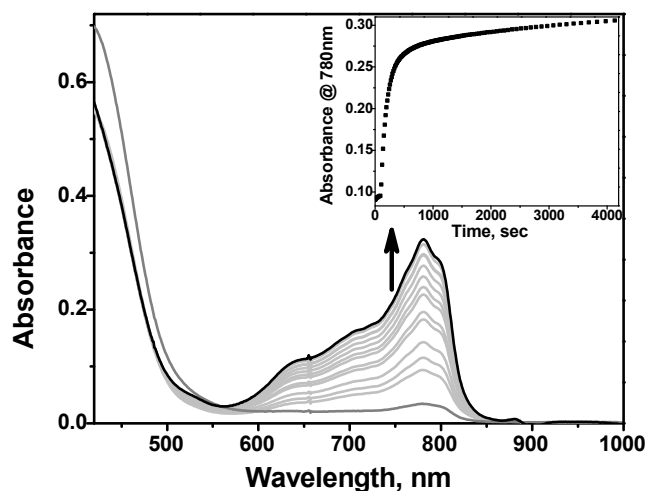## 4. Evaluation of the Catalytic activity of Co₄L1 towards dioxygen reduction:

Figure S7a. Spectral changes associated with the reduction of dioxygen by Fc* (3.0 mM) catalyzed by **Co₄L1** (0.01 mM) in the presence of TFA (10.0 mM) in O_2-saturated acetone (0.18 mM) at -50 °C. Inset: Time trace of the absorption band at 780 nm due to the formation of Fc*$^+$.
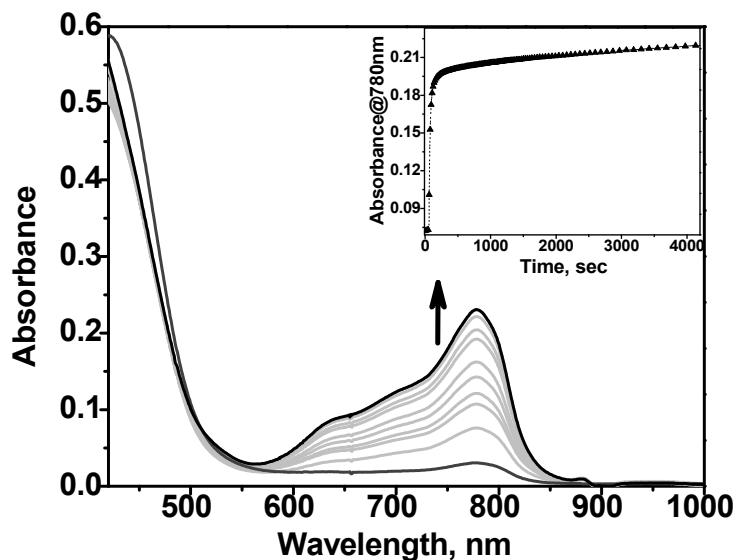

Figure S7b. Spectral changes associated with the reduction of dioxygen by Fc* (3.0 mM) catalyzed by **Co₄L1** (0.01 mM) in the presence of TFA (10.0 mM) in O_2-saturated acetone (0.18 mM) at +25 °C. Inset: Time trace of the absorption band at 780 nm due to the formation of Fc*$^+$.
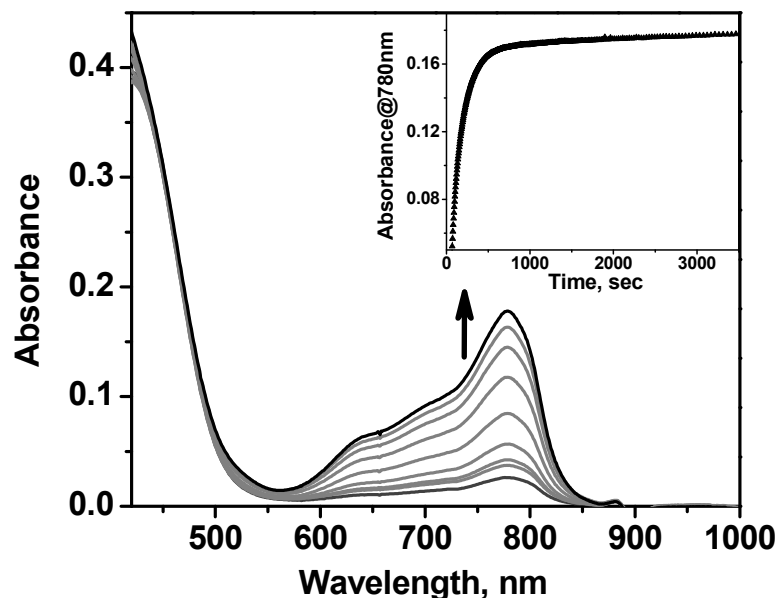
Figure S7c. Spectral changes associated with the reduction of dioxygen by Fc* (3.0 mM) catalyzed by **Co₄L1** (0.01 mM) in the presence of TFA (10.0 mM) in O₂-saturated acetone (0.18 mM) at +30 °C. Inset: Time trace of the absorption band at 780 nm due to the formation of Fc*⁺.

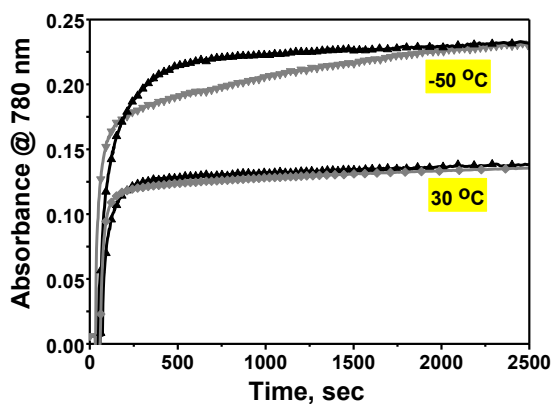**Figure S7d.** Time profiles of the formation of Fc*⁺ monitored at 780 nm during the reduction of O₂ (0.13 mM) by Fc* (3 mM) and **Co₄L1** (0.04 mM) in the presence of TFA (10 mM, black line) and HBF₄ (10 mM, gray line) in acetone at 30 °C as well as at −50 °C.

5. <u>TON calculation for Co₄L1:</u>

TON value was calculated from the moles of Fc*[+] formed divided by the initial moles of the catalyst **Co₄L1** from a reaction mixture containing **Co₄L1**, Fc* and TFA with concentrations of 0.01 mM, 3.0 mM and 10 mM, respectively, in 2 mL of O_2-saturated acetone.
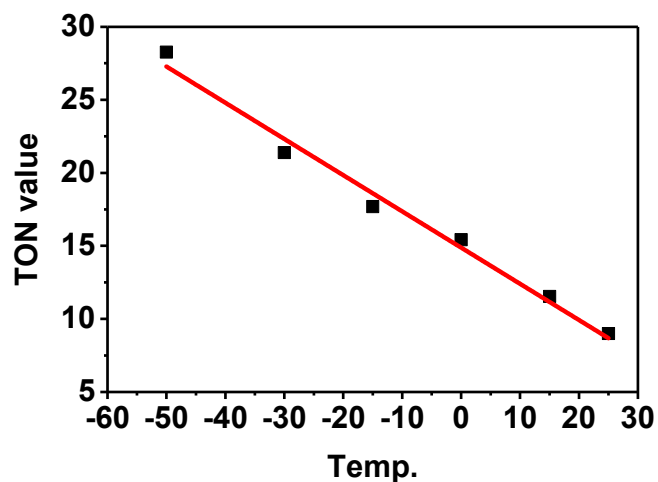

Figure S8. TON vs temperature plot for the **Co₄L1** catalyzed O_2 reduction reaction.

Table S3: Variation of TON as a function of temperature for the **Co₄L1** catalyzed O_2 reduction reaction

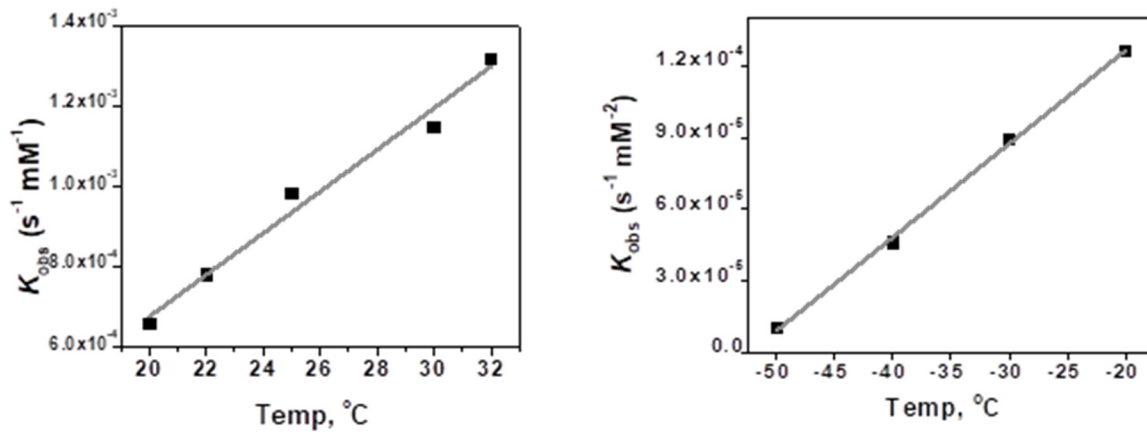| Temp.	[Co₄L]	TON
-50 °C	0.01 mM	28.7
-30 °C	0.01 mM	21.4
-15 °C	0.01 mM	17.7
0 °C	0.01 mM	15.4
+15 °C	0.01 mM	11.5
+25 °C	0.01 mM	9

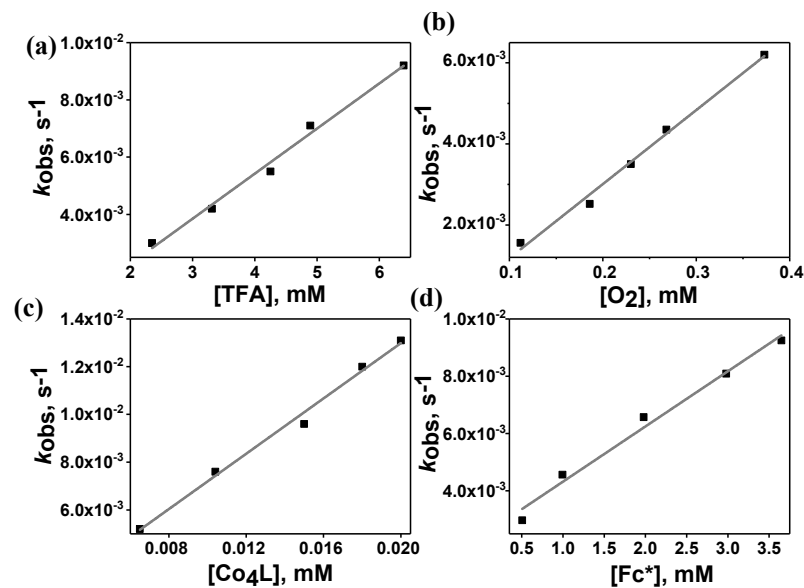**Figure S9.** Variation of the PT (left) and PCET (right) rates as a function of temperature for **Co₄L1**

Figure S10. Studies of the four-electron reduction of O_2 in acetone at -50 °C catalyzed by **Co₄L1**: (a) Plot of k_{obs} vs TFA concentration for the O_2- reduction in O_2-saturated acetone with Fc* (3 mM) catalyzed by **Co₄L1** (0.01 mM) with TFA (2−6.5 mM). (b) Plot of k_{obs} vs [O_2] for the reduction of O_2 (0.1−0.4 mM) with Fc* (3 mM) catalyzed by **Co₄L1** (0.01 mM) with TFA (10 mM). (c) k_{obs} vs [**Co₄L1**] for the O_2-reduction in O_2- saturated acetone (11 mM) with Fc* (3 mM) catalyzed by **Co₄L1** (0.0005− 0.02 mM) with TFA (10 mM). (d) k_{obs} vs [Fc*] for the O_2-reduction in O_2- saturated acetone with Fc* (0.5−3.5 mM) catalyzed by Co₄L1 (0.05 mM) with TFA (10 mM).
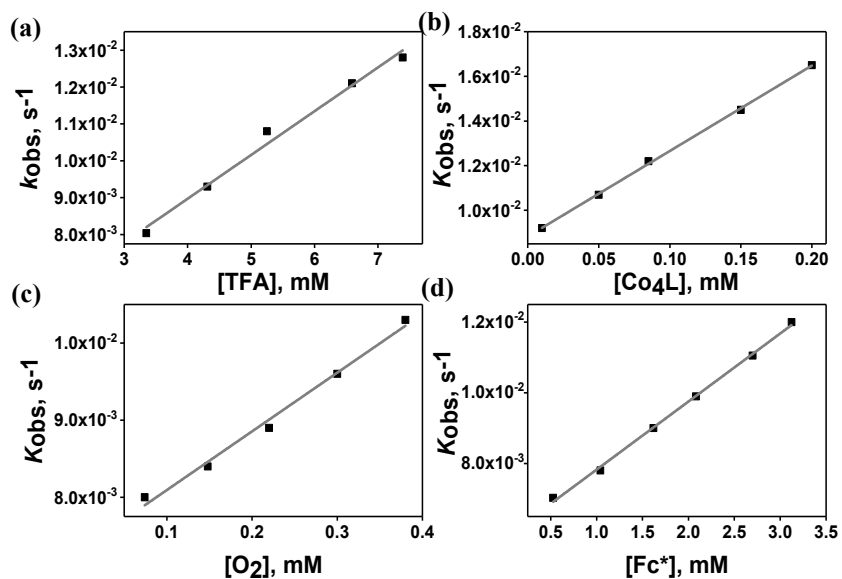
Figure S11. Studies of the two-electron reduction of O_2 in acetone at 25 °C catalyzed by **Co₄L1**: (a) Plot of k_{obs} vs TFA concentration for the O_2- reduction in O_2-saturated acetone with Fc* (3 mM) catalyzed by **Co₄L1** (0.01 mM) with TFA (3−7.5 mM). (b) k_{obs} vs [**Co₄L1**] for the O_2-reduction in O_2- saturated acetone (11 mM) with Fc* (3 mM) catalyzed by **Co₄L1** (0.01− 0.2 mM) with TFA (10 mM). (c) Plot of k_{obs} vs [O_2] for the reduction of O_2 (0.05−0.4 mM) with Fc* (3 mM) catalyzed by **Co₄L1** (0.01 mM) with TFA (10 mM). (d) k_{obs} vs [Fc*] for the O_2-reduction in O_2- saturated acetone with Fc* (0.5−3.5 mM) catalyzed by **Co₄L1** (0.01 mM) with TFA (10 mM).

Table S4. Experimental X-ray diffraction parameters and crystal data for **L1 (CCDC 818335)**

	Tetra Ligand
Empirical formula	$C_{120}H_{156}N_{16}O_{10}Sn_4$
Formula mass	2457.37
Crystal habit, color	Plate, colorless
Crystal dim. (mm)	0.20 x 0.35x 0.40
Crystal system	Triclinic
Space Group	*P-1*
a [Å]	13.1004(6)
b [Å]	15.7386(7)
c [Å]	17.8971(8)
α [°]	65.224(3)
β [°]	70.191(3)
γ [°]	79.065(4)
V [Å^3]	3147.2(2)
Z	1
D [g.cm^{-1}]	1.297
F000	1268
μ(Mo-Kα) [cm^{-1}]	0.844
θ range	3.38-27.00
Refl. collected	37485
Unique refl.	13631
R_{int}	0.0818
Reflections used	9638
Parameters refined	684
R_1	0.0482
wR_2	0.0929
GooF	0.994
Diff. peak/ hole [e/Å^3]	-1.21/1.08

References:

[S1] (a) S. Kundu, E. Matito, S. Walleck, F. F. Pfaff, F. Heims, B. Rabaý, M. J. Luis, A. Company, B. Braun, T. Glaser, K. Ray, *Chem. - Eur. J.* 2012, **18**, 2787 (b) I. Monte-Pérez, S. Kundu, A. Chandra, E. K. Craigo, P. Chernev, U. Kuhlmann, H. Dau, P. Hildebrandt, C. Greco, C. Van Stappen, N. Lehnert, K. Ray, *J. Am. Chem. Soc.* 2017, **139**, 15033– 15042. [c] P. Mialane, A. Nivorojkine, G. Pratviel, L. Azéma, M. Slany, F. Godde, A. Simaan, F. Banse, T. Kargar-Grisel, G. Bouchoux, J. Sainton, O. Horner, J. Guilhem, L. Tchertanova, B. Meunier, J. J. Girerd, Inorg. Chem.1999, 38, 1085-1092.

[S2] Chai, C. L. L.; Armarego, W. L. F. Purification of Laboratory Chemicals, 5th ed.; Butterwirth-Heinemann:New York, 2003.

[S3] (a) L. A. Spek, *J. Appl. Cryst.*2003, **36**, 7. (b) M. G. Sheldrick, *SHELXS-97*, Program for Crystal Structure Solution; University of Göttingen, **1997**.

[S4] M. G. Sheldrick, *SHELXL-97*, Program for Crystal Structure Refinement; University of Göttingen, **1997**.

[S5] A.L. Ankudinov, B. Ravel, J.J. Rehr, S.D.Conradson, *Phys. Rev. B.,* 1998, **58**, 7565–7576.

[S6] H. Dau, P. Liebisch, M. Haumann, *Anal. Bioanal. Chem.,* 2003, **376**, 562–583.

[S7] (a) A.D. Becke, *J. Chem. Phys*., 1993, **98**, 5648–5652. (b) J.P. Perdew, J.A. Chevary, S.H. Vosko, K.A. Jackson, M.R. Pederson, D.J. Singh, C. Fiolhais, *Phys. Rev. B.,* 1992, **46**, 6671–6687.

[S8] (a) M. Dolg, U. Wedig, H. Stoll, H. Preuss, *J. Chem. Phys.* 1987, **86**, 866–872. (b) J.M.L. Martin, A. Sundermann, *J. Chem. Phys.* 2001, **114**, 3408–3420.

[S9] Gaussian 16, Revision C.01, M. J. Frisch, *et al.* Gaussian, Inc., Wallingford CT, **2016**.

[S10] A. Klamt, G. Schüürmann, *J. Chem. Soc., Perkin Trans 2.,* 1993, **5**, 799-805.

[S11] S. Grimme, J. Anthony, S. Ehrlich, H. Krieg, *J. Chem. Phys.* 2010, **132**, 154104.

[S12] R.W.F. Bader, *Atoms in Molecules*. A Quantum Theory; Cambridge University Press: Oxford U.K., **1991**.

[S13] E.R. Johnson, S. Keinan, P. Mori-Sanchez, J. Contreras-García, A.J. Cohen, W. Yang, *J. Am. Chem. Soc.,* 2010, **132**, 6498–6506.

[S14] (a) M. Kohout, *Int. J. Quantum Chem.* 2004, **97**, 651–658. (b) M. Kohout, F.R. Wagner, Y. Grin, *Theor. Chem. Acc.* 2008, **119**, 413–420.

[S15] F. Biegler-König, J. Schönbohm, D. Bayles, *J. Comput. Chem*. 2001, **22**, 545–559.

[S16] M. Kohout, *DGRID*-4.6 Radebeul, **2015**.

[S17] J. Contreras-García, E. Johnson, S. Keinan, R. Chaudret, J.-P. Piquemal, D. Beratan, W. Yang, *J. Chem. Theor. Comp.* 2011, **7**, 625–632.

[S18] C.B. Hübschle, P. Luger, *J. Appl. Crystallogr*. 2006, **39**, 901–904.